Localized dynamic kinetic-energy model for compressible wavelet-based adaptive large-eddy simulation

Giuliano De Stefano [*]
Engineering Department, University of Campania, Aversa, I-81031, Italy

Eric Dymkoski
Adaptive Wavelet Technologies LLC, Louisville, Colorado 80027, USA

Oleg V. Vasilyev
Keldysh Institute of Applied Mathematics of Russian Academy of Sciences, Moscow, 125047, Russia and Adaptive Wavelet Technologies LLC, Louisville, Colorado 80027, USA

(Received 10 November 2021; accepted 9 May 2022; published 24 May 2022)

Wavelet-based adaptive large-eddy simulation (WA-LES) is an extension of the LES method where wavelet threshold filtering is used to separate resolved (more energetic) from residual (less energetic) turbulent flow motions. The effect of unresolved less energetic coherent structures is approximated through deterministic closure models. The method has been recently extended to compressible flows, where the governing equations are expressed in terms of wavelet-based density-weighted Favre-filtered variables. In this study, a novel localized dynamic model for compressible WA-LES of inhomogeneous flows is developed and tested for wall-bounded turbulence. The proposed model, which is based on the solution of the additional evolution equation for the subgrid-scale turbulent kinetic energy, extends the original incompressible formulation in De Stefano *et al.* [Phys. Fluids **20**, 045102 (2008)] to compressible flows. The new modeling procedure is successfully validated for a classical benchmark case that is the supersonic turbulent flow in a plane channel.

DOI: 10.1103/PhysRevFluids.7.054604

I. INTRODUCTION

The accurate modeling of turbulence continues to be one of the major challenges in developing computational technologies capable of effectively predicting the behavior of high Reynolds number flows of engineering interest. Due to the ability to directly resolve flow dependent large scale structures, rather than modeling time or ensemble averaged flow fields as in Reynolds-averaged Navier-Stokes (RANS) approaches [1–3], large-eddy simulation (LES) [4–6] and related methods, such as wall-modeled LES [7–9], detached-eddy simulation (DES) [10,11], and hybrid RANS/LES [12–15], have been gaining more and more popularity in computational fluid dynamics. The main strength of the LES–type approaches is that they mitigate the high-computational cost restrictions of direct numerical simulation (DNS) [16,17], while preserving the ability to accurately predict spatiotemporal characteristics of turbulent flows.

Fluid turbulence is characterized by the existence of coherent energetic eddies that are highly localized and intermittent in both space and scale, yet traditional LES approaches rely on static

[*]giuliano.destefano@unicampania.it

computational meshes that, at best, make use of stretched grids or zonal mesh adaptation. As a result, the flow is often over-resolved in regions between the coherent structures, and under-resolved in regions where localized energetic coherent small-scale structures control the flow dynamics, thus, relying on modeling the effect of unresolved subgrid-scale (SGS) turbulent motions. While a variety of turbulence closures has been proposed [5,6,9,14], most of them consist of deterministic SGS models, which were shown to be dominated by a small number of coherent modes that mainly contribute to SGS dissipation [18]. In fact, the majority of the incoherent SGS modes, due to substantial decorrelation with resolved modes, practically, have very little influence, with negligible contribution to SGS dissipation.

An alternative approach, referred to as wavelet-based adaptive large-eddy simulation (WA-LES), was recently introduced [19,20] adopting a somewhat different philosophy, where, instead of resolving *a priori* defined large scales, dynamically important energetic coherent structures are resolved on a dynamically adaptive computational mesh. The approach fully utilizes spatial/temporal intermittency of turbulent flows and tightly integrates numerics and physics-based modeling. The WA-LES method, which has been recently comprehensively reviewed in Ref. [21], employs a wavelet threshold filter (WTF) to dynamically resolve and track the more energetic, coherent structures during the simulation, while modeling the effect of the unresolved less energetic modes. Similarly to classical LES approaches, the effect of unresolved motions is approximated by means of deterministic closure models, but, due to better resolution of the coherent turbulent eddies, only the effect of less energetic coherent flow structures, which are filtered out, needs to be modeled. In contrast to traditional LES that is based on linear low-pass filtering, WA-LES uses nonlinear WTF that depends on the instantaneous flow realization. Furthermore, the distinctive feature of WA-LES is in the direct coupling between the dynamically adaptive computational grid and the SGS model. In fact, the method has the ability to either compensate for inadequate SGS dissipation provided by the model by increasing the local resolution and, hence, the level of resolved viscous dissipation, or coarsen the mesh in regions of excessive SGS dissipation [22].

Analogously to traditional LES research, where relatively few approaches have been developed for compressible turbulent flows [23–27], most of the efforts in developing WA-LES methodology were concentrated on incompressible flows. Indeed, a number of closure procedures from incompressible LES were extended to WA-LES, including dynamic Smagorinsky model [19], Lagrangian path-line/tube dynamic model [28], and one-equation dynamic models [29]. It is worth noting that, due to the local nature of the WA-LES approach and the use of dynamically adaptive meshes resolving the energetic coherent flow structures, all of the SGS models utilized in WA-LES are localized and do not involve any spatial averaging. These models have been thoroughly assessed for both homogeneous [30,31] and inhomogeneous [22,32] incompressible turbulent flows. A first step towards the construction of SGS models for compressible WA-LES was recently undertaken in Ref. [33], where the unclosed terms in the wavelet-filtered governing equations were approximated by using an eddy-viscosity/conductivity modeling procedure based on the anisotropic minimum-dissipation (AMD) approach [34]. The AMD model, which was properly designed to account for grid anisotropy, has a low computational complexity and gave accurate results in WA-LES of turbulent compressible channel flow.

In this work, a new localized dynamic kinetic-energy model (LDKM) is developed for WA-LES of inhomogeneous compressible turbulent flows. The modeling procedure is based on the classical eddy-viscosity/conductivity assumption, where the model coefficients are expressed in terms of the so-called SGS kinetic energy, for which the evolution equation is derived. The present formulation extends the original WA-LES approach based on LDKM, which was already developed for incompressible flows [29], by following the compressible LES formulation based on local one-equation dynamic kinetic-energy modeling of Chai and Mahesh [26], where WTF is used to derive the exact SGS kinetic-energy transport equation and the LDKM procedure. The compressible LDKM formulation has two properties that make it particularly suitable for compressible WA-LES, namely, its localized nature, which does not require additional volume averaging, and individual dynamic modeling of the different residual terms that are SGS stresses, SGS heat flux, triple

correlation, solenoidal and dilatational dissipations, and pressure dilatation. To establish the viability of the proposed model, as well as its potential application to inhomogeneous flows, the supersonic turbulent flow in a plane channel is considered as a benchmark problem [35].

The rest of the paper is organized as follows. The WA-LES methodology for modeling and simulation of turbulent compressible flows is briefly reviewed in Sec. II. The novel LDKM procedure for compressible WA-LES is introduced and developed in Sec. III, while the dynamic procedure for the determination of the model coefficients is presented in Sec. IV. The results of the application to supersonic channel flow are discussed in Sec. V and, finally, some concluding remarks are drawn in Sec. VI.

II. COMPRESSIBLE WAVELET-BASED ADAPTIVE LARGE-EDDY SIMULATION

In this section, the overall wavelet-based adaptive methodology for the numerical simulation of compressible turbulent flows is presented.

A. Wavelet threshold filtering

Let us briefly outline the main features of WTF, which plays the key-role in WA-LES formulations. A flow field variable, say $\vartheta(\mathbf{x})$, can be represented in terms of wavelet basis functions as

$$\vartheta(\mathbf{x}) = \sum_{\mathbf{l}\in\mathcal{L}^0} c_{\mathbf{l}}^0 \phi_{\mathbf{l}}^0(\mathbf{x}) + \sum_{j=0}^{+\infty}\sum_{\mu=1}^{2^3-1}\sum_{\mathbf{k}\in\mathcal{K}^{\mu,j}} d_{\mathbf{k}}^{\mu,j}\psi_{\mathbf{k}}^{\mu,j}(\mathbf{x}), \tag{1}$$

where $\phi_{\mathbf{l}}^0$ and $\psi_{\mathbf{k}}^{\mu,j}$ are three-dimensional scaling functions and wavelets of different families and levels of resolution, indexed with μ and j, respectively. Indeed, the scaling function coefficients $c_{\mathbf{l}}^0$ represent the averaged values of the field, while the wavelet coefficients $d_{\mathbf{k}}^{\mu,j}$ represent the details of the field itself at different scales. The above wavelet decomposition can be thought as of a multiresolution representation of the variable ϑ, where each level of resolution (except the coarsest one) consists of a family of wavelets $\psi_{\mathbf{k}}^{\mu,j}$ having the same scale but located at different positions.

Wavelet filtering is performed in wavelet space using wavelet coefficient thresholding, which represents a nonlinear filter that depends on each flow realization. Given the number of resolution levels $J_{\max}$, the wavelet thresholding filtered variable is defined by

$$\overline{\vartheta}^{>\epsilon}(\mathbf{x}) = \sum_{\mathbf{l}\in\mathcal{L}^0} c_{\mathbf{l}}^0 \phi_{\mathbf{l}}^0(\mathbf{x}) + \sum_{j=0}^{J_{\max}}\sum_{\mu=1}^{2^3-1}\sum_{\substack{\mathbf{k}\in\mathcal{K}^{\mu,j}\\ |d_{\mathbf{k}}^{\mu,j}|>\epsilon\|\vartheta\|_{\mathrm{WTF}}}} d_{\mathbf{k}}^{\mu,j}\psi_{\mathbf{k}}^{\mu,j}(\mathbf{x}), \tag{2}$$

where $\epsilon > 0$ stands for the nondimensional (relative) threshold parameter, with $\|\cdot\|_{\mathrm{WTF}}$ being the WTF norm providing the (absolute) dimensional scale. For instance, in this work, the dimensional scaling $\|\vartheta\|_{\mathrm{WTF}}$ is specified using the L_2 norm. This way, the filtering operation Eq. (2) is uniquely defined by the parameter ϵ, which stands for the prescribed, uniform threshold.

The major strength of WTF is the ability to compress the numerical solution. For turbulent flow fields, which contain isolated high-energy coherent structures on a low-energy background, most wavelet coefficients are small. Thus, a good approximation of the unfiltered field can be retained even after discarding a large number of wavelets with small coefficients. Intuitively, in the wavelet decomposition Eq. (1), the coefficient $d_{\mathbf{k}}^{\mu,j}$ is small unless the variable ϑ has significant variation on the level of resolution j, in the immediate vicinity of the wavelet $\psi_{\mathbf{k}}^{\mu,j}$ location.

When applying the WTF to the compressible Navier–Stokes equations, each variable should be spatially filtered, according to Eq. (2), with a corresponding absolute scale. But, this strategy would lead to numerical complications, due to the one-to-one correspondence between wavelet locations

and grid points, because each variable should be solved on a different numerical grid. To avoid this difficulty, the coupled wavelet thresholding strategy is employed. Namely, after constructing the various masks of significant wavelet coefficients for each dependent variable, the union of them provides the global thresholding mask that is actually used for all the variables. This way, WTF can be viewed as a local low-pass filtering procedure. Such an interpretation highlights the similarity between WA-LES and conventional LES approaches. However, the wavelet filter is drastically different from the standard LES filters mainly due to its ability to dynamically adapt to the solution. Practically, the WTF-based process generates an adaptive computational grid that tracks the areas of locally significant energy in physical space for the ongoing simulation.

B. Wavelet-filtered compressible Navier-Stokes equations

The governing equations for compressible WA-LES, which describe the evolution of the resolved energetic coherent structures, are formally obtained by applying the WTF procedure to the following balance equations for mass, momentum, and total energy,

$$\frac{\partial \rho}{\partial t} = -\frac{\partial}{\partial x_j}(\rho u_j), \tag{3}$$

$$\frac{\partial}{\partial t}(\rho u_i) = -\frac{\partial}{\partial x_j}(\rho u_i u_j + p\delta_{ij} - \sigma_{ij}) + \rho f_i, \tag{4}$$

$$\frac{\partial}{\partial t}(\rho e) = -\frac{\partial}{\partial x_j}[(\rho e + p)u_j - \sigma_{ij}u_i + q_j] + \rho f_j u_j, \tag{5}$$

where the summation convention over repeated indices applies, while δ_{ij} stands for the Kronecker δ. The body force f_i is assumed uniform in space, with $f_j u_j$ representing the associated power supplied to the fluid flow. Assuming a Newtonian fluid, the viscous shear-stress tensor in Eq. (4) is given by

$$\sigma_{ij} = 2\mu S^*_{ij} = 2\mu\left(S_{ij} - \frac{1}{3}S_{kk}\delta_{ij}\right), \tag{6}$$

wherein S^*_{ij} represents the deviatoric part of the strain rate tensor

$$S_{ij} = \frac{1}{2}\left(\frac{\partial u_i}{\partial x_j} + \frac{\partial u_j}{\partial x_i}\right). \tag{7}$$

The molecular dynamic viscosity is assumed dependent on the temperature, $\mu = \mu(T)$, while the thermodynamic state of the fluid is determined by the ideal-gas equation

$$p = \rho RT, \tag{8}$$

where R is the specific gas constant. The fluid is assumed as a calorically perfect gas, for which the specific heat at constant pressure and the speed of sound are defined as, respectively, $c_p = \gamma R/(\gamma - 1)$ and $a(T) = (\gamma RT)^{1/2}$, with γ being the ratio of specific heats. In Eq. (5), the total energy per unit volume is defined as the sum of internal and kinetic energies, namely,

$$\rho e = \frac{p}{\gamma - 1} + \frac{1}{2}\rho u_i u_i, \tag{9}$$

while the heat flux is defined by

$$q_j = -\lambda\frac{\partial T}{\partial x_j}. \tag{10}$$

The thermal conductivity is dependent on the temperature, $\lambda = \lambda(T)$, according to $\lambda = \mathrm{Pr}^{-1}c_p\mu$, where Pr stands for the molecular Prandtl number that is assumed constant.

Similarly to classical compressible LES formulations, the WA-LES governing equations are written in terms of density-weighted Favre-filtered variables. In this study, the linear Favre-filtering

operator $\widetilde{(\cdot)}$ is defined in conjunction with the WTF operator $\overline{(\cdot)}^{>\epsilon}$ based on the following identity:

$$\overline{\rho\vartheta}^{>\epsilon} = \overline{\rho}^{>\epsilon}\widetilde{\vartheta}, \tag{11}$$

where ϑ stands for a generic flow field variable. Therefore, the wavelet-filtered version of the ideal-gas Eq. (8) reads

$$\overline{p}^{>\epsilon} = \overline{\rho}^{>\epsilon} R\widetilde{T}, \tag{12}$$

with $\widetilde{T}$ representing the resolved Favre-filtered temperature field. By applying the WTF operation to the continuity Eq. (3) and momentum Eq. (4), while assuming that filtering commutes with temporal and spatial derivatives, the following filtered equations are obtained:

$$\frac{\partial \overline{\rho}^{>\epsilon}}{\partial t} = -\frac{\partial}{\partial x_j}(\overline{\rho}^{>\epsilon}\widetilde{u}_j), \tag{13}$$

$$\frac{\partial}{\partial t}(\overline{\rho}^{>\epsilon}\widetilde{u}_i) = -\frac{\partial}{\partial x_j}(\overline{\rho}^{>\epsilon}\widetilde{u}_i\widetilde{u}_j + \overline{p}^{>\epsilon}\delta_{ij} - \hat{\sigma}_{ij}) - \frac{\partial \tau_{ij}}{\partial x_j} + \overline{\rho}^{>\epsilon} f_i. \tag{14}$$

The resolved viscous shear-stress tensor in the filtered momentum equation is defined as

$$\hat{\sigma}_{ij} = 2\widetilde{\mu}\widetilde{S}^*_{ij}, \tag{15}$$

where $\widetilde{\mu} = \mu(\widetilde{T})$ stands for the resolved dynamic viscosity, while $\widetilde{S}^*_{ij}$ represents the deviatoric part of the resolved strain rate tensor. Note that, here and in the following, the hat symbol is not used to indicate filtered variables, but does denote computable quantities.

Owing to the Favre-filtering approach, the filtered continuity Eq. (13) does not contain any unclosed term. On the contrary, the filtered momentum Eq. (14) involves the SGS stresses,

$$\tau_{ij} = \overline{\rho}^{>\epsilon}(\widetilde{u_i u_j} - \widetilde{u}_i\widetilde{u}_j), \tag{16}$$

which represent unknown quantities to be modeled. Note that, in deriving Eq. (14), the residual term $\frac{\partial}{\partial x_j}(\overline{\sigma}^{>\epsilon}_{ij} - \hat{\sigma}_{ij})$ has been omitted, as is usually done in LES, according to the results of *a priori* tests [36].

C. Wavelet-filtered total energy equation

As far as the energy balance is concerned, several different formulations exist in the literature for the filtered energy equation, e.g., Ref. [37]. Here, the balance equation is written for the wavelet-filtered total energy, namely,

$$\overline{\rho}^{>\epsilon}\widetilde{e} = \frac{\overline{p}^{>\epsilon}}{\gamma - 1} + \frac{1}{2}\overline{\rho}^{>\epsilon}\widetilde{u_i u_i}, \tag{17}$$

which is obtained by applying the WTF operator to Eq. (9). The same energy variable can be expressed in terms of resolved momentum as

$$\overline{\rho}^{>\epsilon}\widetilde{e} = \frac{\overline{p}^{>\epsilon}}{\gamma - 1} + \frac{1}{2}\overline{\rho}^{>\epsilon}\widetilde{u}_i\widetilde{u}_i + \overline{\rho}^{>\epsilon}k, \tag{18}$$

where $\overline{\rho}^{>\epsilon}k = \frac{1}{2}\tau_{ii}$, with k being referred to as SGS kinetic energy that is

$$k = \tfrac{1}{2}(\widetilde{u_i u_i} - \widetilde{u}_i\widetilde{u}_i). \tag{19}$$

Straightforwardly, the transport equation for the filtered energy variable Eq. (17) is obtained by applying the WTF operation to the energy Eq. (5). Following Ref. [38], the filtered energy equation can be formally written as

$$\frac{\partial}{\partial t}(\overline{\rho}^{>\epsilon}\widetilde{e}) = -\frac{\partial}{\partial x_j}[(\overline{\rho}^{>\epsilon}\widetilde{e} + \overline{p}^{>\epsilon})\widetilde{u}_j - \hat{\sigma}_{ij}\widetilde{u}_i + \hat{q}_j] - \frac{\partial}{\partial x_j}(\mathcal{Q}_j + \mathcal{J}_j - \mathcal{D}_j) + \overline{\rho}^{>\epsilon} f_j\widetilde{u}_j, \tag{20}$$

where $\hat{q}_j = -\widetilde{\lambda}\frac{\partial \widetilde{T}}{\partial x_j}$, with $\widetilde{\lambda} = \lambda(\widetilde{T})$, stands for the resolved heat flux. Note that, in deriving Eq. (20), the residual term $\frac{\partial}{\partial x_j}(\overline{q_j}^{>\epsilon} - \hat{q}_j)$ has been omitted, as is usually done in LES, according to the results of *a priori* tests [36].

At the right-hand side of Eq. (20), it holds

$$\mathcal{Q}_j + \mathcal{J}_j = \overline{(\rho e + p)u_j}^{>\epsilon} - (\overline{\rho}^{>\epsilon}\widetilde{e} + \overline{p}^{>\epsilon})\widetilde{u}_j, \tag{21}$$

where the SGS heat flux $\mathcal{Q}_j$ and the triple correlation term $\mathcal{J}_j$ are given by

$$\mathcal{Q}_j = c_p\overline{\rho}^{>\epsilon}\left(\widetilde{Tu}_j - \widetilde{T}\widetilde{u}_j\right) \tag{22}$$

and

$$\mathcal{J}_j = \tfrac{1}{2}\overline{\rho}^{>\epsilon}\left(\widetilde{u_i u_i u_j} - \widetilde{u_i u_i}\widetilde{u}_j\right), \tag{23}$$

respectively. These definitions derive form the total energy Eq. (9) and the ideal-gas Eq. (8), supplemented by their filtered counterparts Eqs. (17) and (12). As for the SGS viscous diffusion, which would be exactly expressed as [38]

$$\frac{\partial \mathcal{D}_j}{\partial x_j} = \frac{\partial}{\partial x_j}(\overline{\sigma_{ij}u_i}^{>\epsilon} - \hat{\sigma}_{ij}\widetilde{u}_i), \tag{24}$$

by neglecting the term $\frac{\partial}{\partial x_j}(\overline{\mu S^*_{ij}u_i}^{>\epsilon} - \tilde{\mu}\widetilde{S^*_{ij}u_i})$, the following approximation is actually used in Eq. (20):

$$\frac{\partial \mathcal{D}_j}{\partial x_j} = \frac{\partial}{\partial x_j}[2\tilde{\mu}(\widetilde{S^*_{ij}u_i} - \widetilde{S^*_{ij}}\widetilde{u}_i)] = \frac{\partial}{\partial x_j}\left[\tilde{\mu}\frac{\partial k}{\partial x_j} + \tilde{\mu}\frac{\partial \tau'_{ij}}{\partial x_i}\right] - \varepsilon_d, \tag{25}$$

where $\tau'_{ij} = \tau_{ij}/\overline{\rho}^{>\epsilon}$, for conciseness. The last term at the right-hand side of Eq. (25) that is

$$\varepsilon_d = \frac{\partial}{\partial x_j}\left[\frac{5}{3}\tilde{\mu}\left(\widetilde{u_j\frac{\partial u_i}{\partial x_i}} - \widetilde{u}_j\frac{\partial \widetilde{u}_i}{\partial x_i}\right)\right] \tag{26}$$

can be referred to as SGS dilatational dissipation, since it vanishes in the incompressible limit. In this study, following Ref. [26], this variable is approximated as

$$\varepsilon_d \cong \frac{5}{3}\tilde{\mu}\left[\widetilde{\left(\frac{\partial u_i}{\partial x_i}\right)^2} - \left(\frac{\partial \widetilde{u}_i}{\partial x_i}\right)^2\right]. \tag{27}$$

Finally, based on approximation Eq. (25), the filtered total energy Eq. (20) can be rewritten as

$$\begin{aligned}\frac{\partial}{\partial t}(\overline{\rho}^{>\epsilon}\widetilde{e}) = &-\frac{\partial}{\partial x_j}[(\overline{\rho}^{>\epsilon}\widetilde{e} + \overline{p}^{>\epsilon})\widetilde{u}_j - \hat{\sigma}_{ij}\widetilde{u}_i + \hat{q}_j] - \frac{\partial}{\partial x_j}\left[\mathcal{Q}_j + \mathcal{J}_j - \tilde{\mu}\frac{\partial k}{\partial x_j} - \tilde{\mu}\frac{\partial \tau'_{ij}}{\partial x_i}\right] \\ &- \varepsilon_d + \overline{\rho}^{>\epsilon} f_j \widetilde{u}_j.\end{aligned} \tag{28}$$

As for any other compressible LES approach, suitable closure models are needed to estimate the unknown SGS terms in the wavelet-filtered momentum Eq. (14) and total energy Eq. (28). In the WA-LES framework, the SGS terms account for the effect of unresolved (less energetic) coherent/incoherent structures on the thermofluid dynamics of resolved (more energetic) coherent structures. It is worth noting that, analogously to what happens for LES with nonuniform filter width, there would be a commutation error between filtering and derivative operators, the theoretical effect of which is not considered in deriving the WA-LES equations. In fact, in a practical simulation, a significant number of wavelets below the prescribed thresholding level are retained in the regions of coherent flow structures, due to using the adjacent zone and reconstruction check procedures, which results in a significant reduction of the commutation error [39].

D. Numerical implementation

The compressible WA-LES equations are numerically solved by means of the adaptive anisotropic wavelet collocation (A-AWC) method [40]. This method employs wavelet compression as an integral part of the numerical algorithm such that the solution is obtained with the optimal number of grid points for a given level of accuracy. Briefly, the AWC method is an adaptive, variable-order method for solving partial differential equations with localized structures that continuously change location and size. Since the computational grid automatically adapts to the solution at every step of the time integration process, in both position and scale, the regions of high gradients or localized structures do not need to be known *a priori*. Also, the method is based on the use of second-generation wavelets [41], which allows the order of the numerical scheme to be easily varied, while showing a computational complexity $O(N)$, where N is the number of retained wavelets, which are those with significant coefficients plus nearest neighbours. For further details, the interested reader is referred to Ref. [39], for instance.

The A-AWC formulation is an extension of the original method developed for general curvilinear coordinate systems, which preserves active error-controlling properties. By separating the computational space from the physical one, while introducing a mapping between the two different spaces, this improved method provides additional flexibility to control mesh anisotropy and solve the problem in complex physical domains. At the same time, the structured rectilinear assembly of collocation points in the computational space may be maintained, thus allowing the use of computationally efficient discrete adaptive wavelet transform and derivative approximations.

III. LOCALIZED DYNAMIC KINETIC-ENERGY EQUATION MODEL

As the coherent part of the unresolved SGS quantities dominates the effect on the evolution of the resolved fields [18], deterministic closure models are presumed to capture this effect in a similar fashion as for incompressible WA-LES. The new LDKM procedure for compressible WA-LES is developed taking into account the corresponding approach proposed for conventional LES [26]. The proposed modeling procedure provides a localized dynamic estimation of the SGS effects, while taking full advantage of the WA-LES adaptivity for complex turbulent flows, without performing any spatial averaging. Furthermore, it exhibits attractive convergence properties, whereby the modeled terms are implicitly coupled to the prescribed WTF level, while automatically vanishing in well resolved or laminar flow regions.

SGS energy-based models were first proposed in Ref. [42] as variations on the dynamic Smagorinsky model that explicitly track a budget of the SGS kinetic-energy Eq. (19), enabling localized computation of SGS terms, while ensuring the numerical stability of the calculations. In fact, originally, spatial averaging was used to compute SGS model coefficients and maintain stability, which limited the application of LES to complex turbulent flows. To compute SGS terms locally and dynamically, LDKM exploits the SGS kinetic energy through resolving an additional transport equation. In the WA-LES context, the LDKM was already developed and successfully implemented for incompressible flows in Ref. [29], while its extension to compressible flow is the subject of the present work.

A. SGS kinetic-energy equation

Differently from other studies, where the compressible SGS kinetic-energy equation stands for a modeled equation that is adapted from the transport equation for turbulent kinetic energy [43], here, this equation is formally derived by properly combining the unfiltered and filtered momentum equations, while exploiting the continuity equation. Following Ref. [26], the SGS kinetic-energy equation is written as

$$\frac{\partial(\overline{\rho}^{>\epsilon}k)}{\partial t} = -\frac{\partial}{\partial x_j}\left[\overline{\rho}^{>\epsilon}k\widetilde{u}_j - \tau_{ij}\widetilde{u}_i - \widetilde{\mu}\frac{\partial k}{\partial x_j} - \widetilde{\mu}\frac{\partial \tau'_{ij}}{\partial x_i} - \frac{\gamma-1}{\gamma}\mathcal{Q}_j + \mathcal{J}_j\right] - \varepsilon_d - \varepsilon_s + \Pi + \mathcal{P}, \quad (29)$$

where WTF takes the place of the spatial filtering operation in the original formulation. Besides the terms that were already introduced above, the other three unknown terms at the right-hand side of Eq. (29) are defined as follows. The SGS solenoidal dissipation rate is given by

$$\varepsilon_{\mathrm{s}} = 2\widetilde{\mu}(\widetilde{S^*_{ij}S^*_{ij}} - \widetilde{S}^*_{ij}\widetilde{S}^*_{ij}), \tag{30}$$

where the deviatoric part of the strain rate tensor Eq. (7) is involved. This variable represents an approximation of the SGS viscous dissipation that is $\varepsilon_{\mathrm{v}} = \overline{\sigma_{ij}S_{ij}}^{\gg\epsilon} - \hat{\sigma}_{ij}\widetilde{S}_{ij}$ [38], which is perfectly consistent with similar approximations discussed in Sec. II C. Moreover, the SGS pressure-dilatation term is defined as

$$\Pi = \overline{p\frac{\partial u_i}{\partial x_i}}^{\gg\epsilon} - \overline{p}^{\gg\epsilon}\frac{\partial \widetilde{u}_i}{\partial x_i}, \tag{31}$$

which clearly vanishes in the incompressible limit. Finally, the SGS kinetic-energy production is given by

$$\mathcal{P} = -\tau_{ij}\widetilde{S}_{ij}, \tag{32}$$

representing the energy transfer (back and forth) between resolved and SGS modes.

Since the evolution of the SGS kinetic energy is explicitly simulated by means of Eq. (29), the computable total energy can be defined in terms of the resolved kinetic energy as follows [36]:

$$\overline{\rho}^{\gg\epsilon}\hat{e} = \frac{\overline{p}^{\gg\epsilon}}{\gamma - 1} + \frac{1}{2}\overline{\rho}^{\gg\epsilon}\widetilde{u}_i\widetilde{u}_i. \tag{33}$$

In fact, according to Eq. (18), the filtered total energy, $\overline{\rho e}^{\gg\epsilon} = \overline{\rho}^{\gg\epsilon}\hat{e} + \overline{\rho}^{\gg\epsilon}k$, results in being the sum of filtered internal energy, resolved kinetic energy, and SGS kinetic energy. Therefore, the balance equation for the computable total energy can be derived by combining Eqs. (28) and (29), thus, obtaining

$$\begin{aligned}\frac{\partial}{\partial t}(\overline{\rho}^{\gg\epsilon}\hat{e}) = &-\frac{\partial}{\partial x_j}[(\overline{\rho}^{\gg\epsilon}\hat{e} + \overline{p}^{\gg\epsilon})\widetilde{u}_j - \hat{\sigma}_{ij}\widetilde{u}_i + \hat{q}_j] \\ &- \frac{\partial}{\partial x_j}(\tau_{ij}\widetilde{u}_i) - \frac{1}{\gamma}\frac{\partial \mathcal{Q}_j}{\partial x_j} + \varepsilon_{\mathrm{s}} - \Pi - \mathcal{P} + \overline{\rho}^{\gg\epsilon}f_j\widetilde{u}_j.\end{aligned} \tag{34}$$

The compressible WA-LES Eqs. (13), (14), (34), and (29) represent a set of unclosed equations in the variables $\overline{\rho}^{\gg\epsilon}$, $\overline{\rho}^{\gg\epsilon}\widetilde{u}_i$, $\overline{\rho}^{\gg\epsilon}\hat{e}$, and $\overline{\rho}^{\gg\epsilon}k$, which are solved with the A-AWC methodology. In particular, the global thresholding mask for WTF is constructed by considering all these flow variables. It is worth noting that the solution of the additional transport equation for the SGS kinetic energy is not computationally expensive because several terms appearing in Eq. (29) are already present in the filtered total energy Eq. (34), besides SGS stresses and SGS heat flux [44]. Also note that, after expressing the filtered pressure field $\overline{p}^{\gg\epsilon}$ in terms of resolved variables by exploiting Eq. (33), the resolved temperature field $\widetilde{T}$ is determined according to the filtered ideal-gas Eq. (12), so that the coefficients $\widetilde{\mu}$ and $\widetilde{\lambda}$ can be evaluated.

B. Compressible WA-LES closure

The compressible WA-LES equations involve a number of unknown SGS terms that need to be modeled. In this work, the following approximations are introduced. The unknown SGS stress tensor Eq. (16) appearing in Eq. (14) is modeled according to

$$\tau_{ij} \cong -2\overline{\rho}^{\gg\epsilon}\nu_e\widetilde{S}^*_{ij} + \tfrac{2}{3}\overline{\rho}^{\gg\epsilon}k\delta_{ij}, \tag{35}$$

where the (traceless) deviatoric part is approximated by adopting the classical eddy-viscosity modeling assumption, while the isotropic part is directly expressed in terms of the solution of the SGS kinetic-energy Eq. (29). By assuming the square root of k as the velocity scale and the WTF

characteristic local width Δ as the length scale for the turbulent eddy-viscosity definition [42], it holds

$$\nu_e = C_\nu \Delta \sqrt{k}, \tag{36}$$

where the dimensionless model coefficient C_ν has to be determined. It is worth noting that the filter width Δ, being a function of the local spatial resolution, has a key role in the WA-LES formulation, strictly reflecting the adaptive nature of the method. Practically, given the prescribed wavelet threshold ϵ, the corresponding thresholding mask implicitly defines a pointwise variable time-dependent filter width. This is completely different from classical nonadaptive LES, where the local, possibly nonuniform, filter width is defined *a priori* and does not depend on the actual flow realization. Naturally, the approximation Eq. (35) is also employed to model the unknown SGS terms involving τ_{ij} in the energy Eqs. (29) and (34). In particular, this holds for the production term $\mathcal{P}$ that appears, with opposite signs, in both of the equations.

As for the residual unclosed terms in the energy equations, in this work, the contribution of each term is approximated separately, instead of being grouped and modeled together, as is often made in other SGS energy-based modeling procedures, e.g., Ref. [25]. Both energy equations are supplied with the eddy-diffusivity model for the unknown SGS heat flux, namely,

$$\mathcal{Q}_j \cong -\lambda_e \frac{\partial \widetilde{T}}{\partial x_j}, \tag{37}$$

where λ_e represents the unknown eddy-conductivity coefficient. The latter parameter can be determined as $\lambda_e = \mathrm{Pr}_t^{-1} c_p \overline{\rho}^{>\epsilon} \nu_e$, where Pr_t stands for the turbulent Prandtl number. Differently from what is usually done in analogous compressible LES applications [45], here, the turbulent Prandtl number is not assumed constant. Therefore, combining with Eq. (36), the turbulent eddy-conductivity can be written as

$$\lambda_e = C_\lambda c_p \overline{\rho}^{>\epsilon} \Delta \sqrt{k}, \tag{38}$$

with C_λ representing the second model coefficient to be determined. Following Ref. [26], the triple correlation Eq. (23) and the SGS pressure-dilatation Eq. (31) terms are approximated, respectively, as

$$\mathcal{J}_j \cong C_J \Delta \overline{\rho}^{>\epsilon} k^{1/2} \frac{\partial k}{\partial x_j} \tag{39}$$

and

$$\Pi \cong C_\Pi \Delta^2 \frac{\partial \overline{p}^{>\epsilon}}{\partial x_j} \frac{\partial}{\partial x_j} \left(\frac{\partial \widetilde{u}_i}{\partial x_i} \right), \tag{40}$$

where C_J and C_Π stand for additional model coefficients. Moreover, using simple scaling arguments [42], the following approximation is used for the SGS solenoidal dissipation rate Eq. (30):

$$\varepsilon_\mathrm{s} \cong C_{\varepsilon_\mathrm{s}} \Delta^{-1} \overline{\rho}^{>\epsilon} k^{3/2}, \tag{41}$$

with $C_{\varepsilon_\mathrm{s}}$ representing a further model coefficient. Finally, the unknown SGS dilatational dissipation rate Eq. (27) can be modeled by being related to the SGS solenoidal dissipation rate as follows:

$$\varepsilon_d = C_d M_t^2 \varepsilon_\mathrm{s}, \tag{42}$$

where the SGS turbulent Mach number is defined by $M_t = \sqrt{2k}/\widetilde{a}$, with $\widetilde{a} = a(\widetilde{T})$, and C_d is a constant of order unity [46]. Practically, combining with Eq. (41), the following approximation is employed in this work:

$$\varepsilon_d \cong 2 C_{\varepsilon_d} \Delta^{-1} \overline{\rho}^{>\epsilon} k^{5/2} \widetilde{a}^{-2}, \tag{43}$$

where C_{ε_d} represents another model coefficient. In the end, the proposed LDKM procedure involves six model coefficients, namely, C_ν, C_λ, C_J, C_Π, C_{ε_s}, and C_{ε_d}, which need to be determined.

IV. DYNAMIC MODELING PROCEDURE

A fully dynamic version of the kinetic-energy equation model for compressible WA-LES, with the model coefficients not prescribed but dynamically derived from the resolved fields, is proposed. The model coefficients C_ν, C_λ and C_J are determined following a Germano-like dynamic approach [4,47], by test-filtering the resolved WA-LES fields and assuming some scale similarity or analogy relationship. This particular implementation of LDKM follows that one proposed in standard LES studies [23,26].

Here, differently from previous works for incompressible WA-LES, where the WTF at twice the threshold was employed, a local low-pass filter is used for test-filtering. Specifically, a discrete low-pass test-filter is constructed using the adjacent grid-points, while ensuring the filter weights positivity and a proper filter width $\widehat{\Delta} = \alpha\Delta$, where $\alpha > 1$ is a constant coefficient of proportionality. By super-imposing the secondary filter, the test-filtered quantity is formally denoted as either $\widehat{\overline{\vartheta}^{>\epsilon}}$ or $\{\widehat{\overline{\vartheta}^{>\epsilon}}\}$, with ϑ representing a generic flow field variable. Thus, at the test-scale level, the associated density-weighted Favre-filtered variable, say $\breve{\breve{\vartheta}}$, is defined by

$$\widehat{\overline{\rho}^{>\epsilon}}\breve{\breve{\vartheta}} = \widehat{\overline{\rho\vartheta}^{>\epsilon}}. \tag{44}$$

At the same level, the resolved total energy becomes: $\frac{\widehat{\overline{p}^{>\epsilon}}}{\gamma-1} + \frac{1}{2}\widehat{\overline{\rho}^{>\epsilon}}\breve{\tilde{u}}_i\breve{\tilde{u}}_i$, while the ideal-gas equation reads: $\widehat{\overline{p}^{>\epsilon}} = \widehat{\overline{\rho}^{>\epsilon}}R\breve{\breve{T}}$, from which the temperature variable $\breve{\breve{T}}$ can be evaluated.

By applying the test-filtering operation upon the momentum Eq. (4), the corresponding residual, subtest-scale (STS) stresses are given by

$$T_{ij} = \widehat{\overline{\rho}^{>\epsilon}}(\widehat{\tilde{u}_i\tilde{u}_j} - \breve{\tilde{u}}_i\breve{\tilde{u}}_j). \tag{45}$$

Test filtering Eq. (16) and combining with Eq. (45), results in the following Germano-like identity:

$$T_{ij} - \widehat{\tau}_{ij} = \mathcal{L}_{ij}, \tag{46}$$

where

$$\mathcal{L}_{ij} = \left\{ \frac{\overline{\rho u_i}^{>\epsilon}\,\overline{\rho u_j}^{>\epsilon}}{\overline{\rho}^{>\epsilon}} \right\} - \frac{\widehat{\overline{\rho u_i}^{>\epsilon}}\,\widehat{\overline{\rho u_j}^{>\epsilon}}}{\widehat{\overline{\rho}^{>\epsilon}}} \tag{47}$$

represent the exact Leonard stresses. These stresses are directly computable from the resolved fields and can be exploited to determine the unknown eddy-viscosity model coefficient as follows. As an analog of Eq. (19), the unresolved kinetic energy at the test-scale level, which is referred to as STS kinetic energy, is defined by

$$k_{\text{sts}} = \tfrac{1}{2}(\widehat{\tilde{u}_i\tilde{u}_i} - \breve{\tilde{u}}_i\breve{\tilde{u}}_i), \tag{48}$$

that is $\widehat{\overline{\rho}^{>\epsilon}}k_{\text{sts}} = \frac{1}{2}T_{ii}$. This way, analogous to Eq. (46), the following identity for the kinetic-energy variables holds:

$$\widehat{\overline{\rho}^{>\epsilon}}k_{\text{sts}} - \widehat{\overline{\rho}^{>\epsilon}}k = \tfrac{1}{2}\mathcal{L}_{ii}, \tag{49}$$

which allows for the STS kinetic energy to be directly expressed in terms of resolved quantities. Based on the eddy-viscosity assumption for the deviatoric SGS stresses, which can be written as

$$\tau^*_{ij} \cong -2C_\nu\Delta\overline{\rho}^{>\epsilon}k^{1/2}\widetilde{S}^*_{ij}, \tag{50}$$

a similar approximation for the deviatoric STS stresses is employed, namely,

$$T^*_{ij} \cong -2C_\nu\widehat{\Delta}\widehat{\overline{\rho}^{>\epsilon}}k^{1/2}_{\text{sts}}\breve{\breve{S}}^*_{ij}, \tag{51}$$

where the model coefficient is assumed to be independent of the filtering level. Test filtering Eq. (50) and combining with Eq. (51), while taking into account Eq. (47), results in

$$\mathcal{L}^*_{ij} = 2C_\nu \mathcal{M}^*_{ij}, \tag{52}$$

where

$$\mathcal{M}^*_{ij} = \{\Delta\overline{\rho}^{>\epsilon} k^{1/2} \widetilde{S^*_{ij}}\} - \widehat{\Delta}\widehat{\overline{\rho}^{>\epsilon}} k_{\rm sts}^{1/2} \breve{\breve{S}}^*_{ij} \tag{53}$$

stand for the modeled Leonard stresses. Solving the over-specification in Eq. (52) by means of a least-square method to minimize the error [47], the space-time dependent model coefficient C_ν is finally determined as

$$C_\nu = \frac{1}{2} \frac{\mathcal{L}^*_{ij} \mathcal{M}^*_{ij}}{\mathcal{M}^*_{ln} \mathcal{M}^*_{ln}}. \tag{54}$$

One of the main advantages of the proposed procedure is that negative values for C_ν are permitted, thus emulating the local SGS turbulent kinetic-energy backscatter, which is the transfer of kinetic energy from unresolved to resolved motions [48]. The inherent instability due to the possible negative SGS dissipation is practically limited by the local budget of SGS kinetic energy that is explicitly taken into account by the modeling process.

A fully dynamic version of the kinetic-energy-based eddy-conductivity model Eq. (38), with the model coefficient not prescribed but derived from the resolved fields, is similarly developed by combining the approximations for SGS and STS heat fluxes that are, respectively,

$$\overline{\rho}^{>\epsilon} (\widetilde{T u_j} - \widetilde{T}\widetilde{u}_j) \cong -C_\lambda \Delta \overline{\rho}^{>\epsilon} k^{1/2} \frac{\partial \widetilde{T}}{\partial x_j} \tag{55}$$

and

$$\widehat{\overline{\rho}^{>\epsilon}} (\breve{\widetilde{T u_j}} - \breve{\widetilde{T}}\breve{\widetilde{u}}_j) \cong -C_\lambda \widehat{\Delta}\widehat{\overline{\rho}^{>\epsilon}} k_{\rm sts}^{1/2} \frac{\partial \breve{\widetilde{T}}}{\partial x_j}, \tag{56}$$

where, again, the same model coefficient is assumed. Test filtering Eq. (55) and combining with Eq. (56), results in the following Germano-like vector identity:

$$\{\, \overline{\rho}^{>\epsilon} \widetilde{u}_j \widetilde{T} \,\} - \widehat{\overline{\rho}^{>\epsilon}} \breve{\widetilde{u}}_j \breve{\widetilde{T}} = C_\lambda \left[\left\{ \Delta \overline{\rho}^{>\epsilon} k^{1/2} \frac{\partial \widetilde{T}}{\partial x_j} \right\} - \widehat{\Delta}\widehat{\overline{\rho}^{>\epsilon}} k_{\rm sts}^{1/2} \frac{\partial \breve{\widetilde{T}}}{\partial x_j} \right], \tag{57}$$

which can be formally written as $L_j = C_\lambda M_j$, where L_j and M_j stand for exact and modeled Leonard-type vector fields, respectively. Solving the over-specification by means of a least-square method to minimize the error [47], the model coefficient C_λ is finally determined as

$$C_\lambda = \frac{L_i M_i}{M_j M_j}. \tag{58}$$

As for the triple correlation term, the following approximations are used at the grid and test-scale levels:

$$\frac{1}{2} \overline{\rho}^{>\epsilon} (\widetilde{u_i u_i u_j} - \widetilde{u_i u_i} \widetilde{u}_j) \cong C_J \Delta \overline{\rho}^{>\epsilon} k^{1/2} \frac{\partial k}{\partial x_j} \tag{59}$$

and

$$\frac{1}{2} \widehat{\overline{\rho}^{>\epsilon}} (\breve{\widetilde{u_i u_i u_j}} - \breve{\widetilde{u_i u_i}} \breve{\widetilde{u}}_j) \cong C_J \widehat{\Delta}\widehat{\overline{\rho}^{>\epsilon}} k_{\rm sts}^{1/2} \frac{\partial k_{\rm sts}}{\partial x_j}, \tag{60}$$

where, again, the same model coefficient is assumed. By test filtering Eq. (59) and combining with Eq. (60), one gets the following Germano-like vector identity:

$$\frac{1}{2}\{\overline{\rho}^{>\epsilon}\widetilde{u_i}\widetilde{u_i}\widetilde{u}_j\} - \frac{1}{2}\widehat{\overline{\rho}^{>\epsilon}}\breve{\widetilde{u_i}}\breve{\widetilde{u_i}}\breve{\widetilde{u}}_j = C_J\left(\widehat{\Delta}\widehat{\overline{\rho}^{>\epsilon}}k_{\rm sts}^{1/2}\frac{\partial k_{\rm sts}}{\partial x_j} - \left\{\Delta\overline{\rho}^{>\epsilon}k^{1/2}\frac{\partial k}{\partial x_j}\right\}\right), \tag{61}$$

which is rewritten as $l_j = C_J m_j$, from which the model coefficient C_J can be dynamically evaluated as

$$C_J = \frac{l_i m_i}{m_j m_j}. \tag{62}$$

Analogously, the model coefficient for the SGS pressure-dilatation in Eq. (40) can be determined based on the following two approximations:

$$\overline{p\frac{\partial u_i}{\partial x_i}}^{>\epsilon} - \overline{p}^{>\epsilon}\frac{\partial\widetilde{u}_i}{\partial x_i} \cong C_\Pi\Delta^2\frac{\partial\overline{p}^{>\epsilon}}{\partial x_j}\frac{\partial^2\widetilde{u}_i}{\partial x_j\partial x_i} \tag{63}$$

and

$$\widehat{\overline{p\frac{\partial u_i}{\partial x_i}}^{>\epsilon}} - \widehat{\overline{p}^{>\epsilon}}\frac{\partial\breve{\widetilde{u}}_i}{\partial x_i} \cong C_\Pi\widehat{\Delta}^2\frac{\partial\widehat{\overline{p}^{>\epsilon}}}{\partial x_j}\frac{\partial^2\breve{\widetilde{u}}_i}{\partial x_j\partial x_i}, \tag{64}$$

where, once again, the same model coefficient is assumed. By test filtering Eq. (63) and combining with Eq. (64), one obtains the following Germano-like scalar identity:

$$\{\overline{p}^{>\epsilon}\frac{\partial\widetilde{u}_i}{\partial x_i}\} - \widehat{\overline{p}^{>\epsilon}}\frac{\partial\breve{\widetilde{u}}_i}{\partial x_i} = C_\Pi\left(\widehat{\Delta}^2\frac{\partial\widehat{\overline{p}^{>\epsilon}}}{\partial x_j}\frac{\partial^2\breve{\widetilde{u}}_i}{\partial x_j\partial x_i} - \left\{\Delta^2\frac{\partial\overline{p}^{>\epsilon}}{\partial x_j}\frac{\partial^2\widetilde{u}_i}{\partial x_j\partial x_i}\right\}\right), \tag{65}$$

from which the model coeffient C_Π is directly estimated.

As for the determination of the model coefficients for the SGS energy dissipation rates that are C_{ε_s} and C_{ε_d}, a Bardina-like approach is followed [29,49], because the Germano-like approach was shown to provide underestimated values [24,50]. According to definitions Eqs. (30) and (27), the resolved solenoidal and dilatational dissipation rates at the test-scale level are, respectively,

$$\mathcal{E}_{\rm s} = 2\{\widetilde{\mu}\widetilde{S}_{ij}^*\widetilde{S}_{ij}^*\} - 2\breve{\widetilde{\mu}}\breve{\widetilde{S}}_{ij}^*\breve{\widetilde{S}}_{ij}^* \tag{66}$$

and

$$\mathcal{E}_d = \frac{5}{3}\left\{\widetilde{\mu}\left(\frac{\partial\widetilde{u}_i}{\partial x_i}\right)^2\right\} - \frac{5}{3}\breve{\widetilde{\mu}}\left(\frac{\partial\breve{\widetilde{u}}_i}{\partial x_i}\right)^2, \tag{67}$$

where $\breve{\widetilde{\mu}} = \mu(\breve{\widetilde{T}})$. By analogy with approximations Eqs. (41) and (43), these quantities can be evaluated as, respectively,

$$\mathcal{E}_{\rm s} = C_{\varepsilon_s}\widehat{\Delta}^{-1}\widehat{\overline{\rho}^{>\epsilon}}k_{\rm sts}^{3/2} \tag{68}$$

and

$$\mathcal{E}_d = 2C_{\varepsilon_d}\widehat{\Delta}^{-1}\widehat{\overline{\rho}^{>\epsilon}}k_{\rm sts}^{5/2}\breve{\widetilde{a}}^{-2}, \tag{69}$$

where $\breve{\widetilde{a}} = a(\breve{\widetilde{T}})$, from which the two unknown model coefficients are directly determined.

V. APPLICATION TO SUPERSONIC CHANNEL FLOW

The compressible WA-LES approach supplied with the LDKM procedure is specifically designed to simulate complex inhomogeneous turbulent flows. The present study evaluates the proposed method for a classical benchmark problem that is the turbulent supersonic flow in a plane channel with isothermal walls.

A. Case study

The present flow geometry is based on the pioneering DNS studies of Coleman and co-authors [35,51], where the size of the computational domain is given as $4\pi H \times 2H \times 4\pi H/3$, with H representing the channel half-height. The spatial coordinates, denoted as either (x_1, x_2, x_3) or (X, Y, Z), are aligned with the streamwise, wall-normal, and spanwise directions, respectively, where $x_2 = 0$ corresponds to the midplane of the channel. Periodic boundary conditions are applied along the two homogeneous directions that are x_1 and x_3, while no-slip conditions for the velocity and the constant temperature of $T_w = 293.15\ K$ are imposed at the cooled walls of the channel $(x_2/H = \pm 1)$.

Fully developed flow conditions are achieved by sustaining the flow through external uniform body forcing in the streamwise direction [51], similar to what was done in other LES studies [45], where the forcing level is determined as follows. Theoretically, by averaging the streamwise momentum Eq. (14) on the homogeneous plane, it holds

$$\frac{\partial}{\partial t}[\overline{\rho}^{>\epsilon}\widetilde{u}_1]_{XZ} = -\frac{\partial}{\partial Y}[\overline{\rho}^{>\epsilon}\widetilde{u}_1\widetilde{u}_2 - \hat{\sigma}_{12} + \tau_{12}]_{XZ} + [\overline{\rho}^{>\epsilon}]_{XZ} f_i \delta_{i1}, \tag{70}$$

where $[\cdot]_{XZ}$ denotes plane averaging. Defining the mean bulk mass flux and density as

$$(\rho U)_b = \frac{1}{2H}\int_{-H}^{H} [\overline{\rho}^{>\epsilon}\widetilde{u}_1]_{XZ} dY \tag{71}$$

and

$$\rho_b = \frac{1}{2H}\int_{-H}^{H} [\overline{\rho}^{>\epsilon}]_{XZ} dY, \tag{72}$$

respectively, by further averaging Eq. (70) along the wall-normal direction, the relation

$$\frac{d}{dt}(\rho U)_b = -\frac{\tau_w}{H} + \rho_b f_1 \tag{73}$$

is obtained. Therefore, by imposing a steady condition for the bulk mass flux, the time-dependent body force intensity results in being directly related to the averaged wall shear stress, namely $f_1(t) = \frac{\tau_w}{\rho_b H}$. Practically, following Ref. [33], the forcing variable f_1 is evolved in time according to a simple feedback control equation that is

$$\frac{df_1}{dt} = \left[1 - \frac{(\rho U)_b}{(\rho U)_b^0}\right]\frac{f_1}{\tau_f}, \tag{74}$$

where $(\rho U)_b^0$ is the imposed goal value, with τ_f being a suitable relaxation time parameter. This way, during the simulation, the time-dependent body force is increased when the instantaneous mean bulk mass flux is lower than prescribed, and viceversa.

The higher Mach number case presented in Ref. [35] is chosen here as the benchmark flow, where significant thermodynamic variations of the fluid properties are present. Specifically, the bulk Mach and Reynolds numbers are $\mathrm{Ma} = U_b/a_w = 3$ and $\mathrm{Re} = (\rho U)_b H/\mu_w = 4880$, where $U_b = (\rho U)_b/\rho_b$, while $a_w = a(T_w)$ and $\mu_w = \mu(T_w) = 1.81 \times 10^{-5}$ kg m^{-1}s^{-1}. Considering ideal gas air conditions, the specific heat ratio $\gamma = 7/5$ and the gas constant $R = 287$ J kg^{-1}K^{-1} are assumed. Moreover, the dependence of the dynamic viscosity on the temperature is given by the Sutherland's law, which is normalized as follows:

$$\frac{\mu(T)}{\mu_w} = \frac{T_w + S_1}{T + S_1}\left(\frac{T}{T_w}\right)^{3/2}, \tag{75}$$

where $S_1 = 110.4\ K$. Also, the molecular Prandtl number $\mathrm{Pr} = 0.72$ is prescribed.

The WA-LES solution is examined in terms of friction Reynolds number, $\mathrm{Re}_\tau = \rho_w u_\tau H/\mu_w$, friction Mach number, $\mathrm{Ma}_\tau = u_\tau/a_w$, and heat flux coefficient, $-B_q = T_\tau/T_w$. The friction velocity

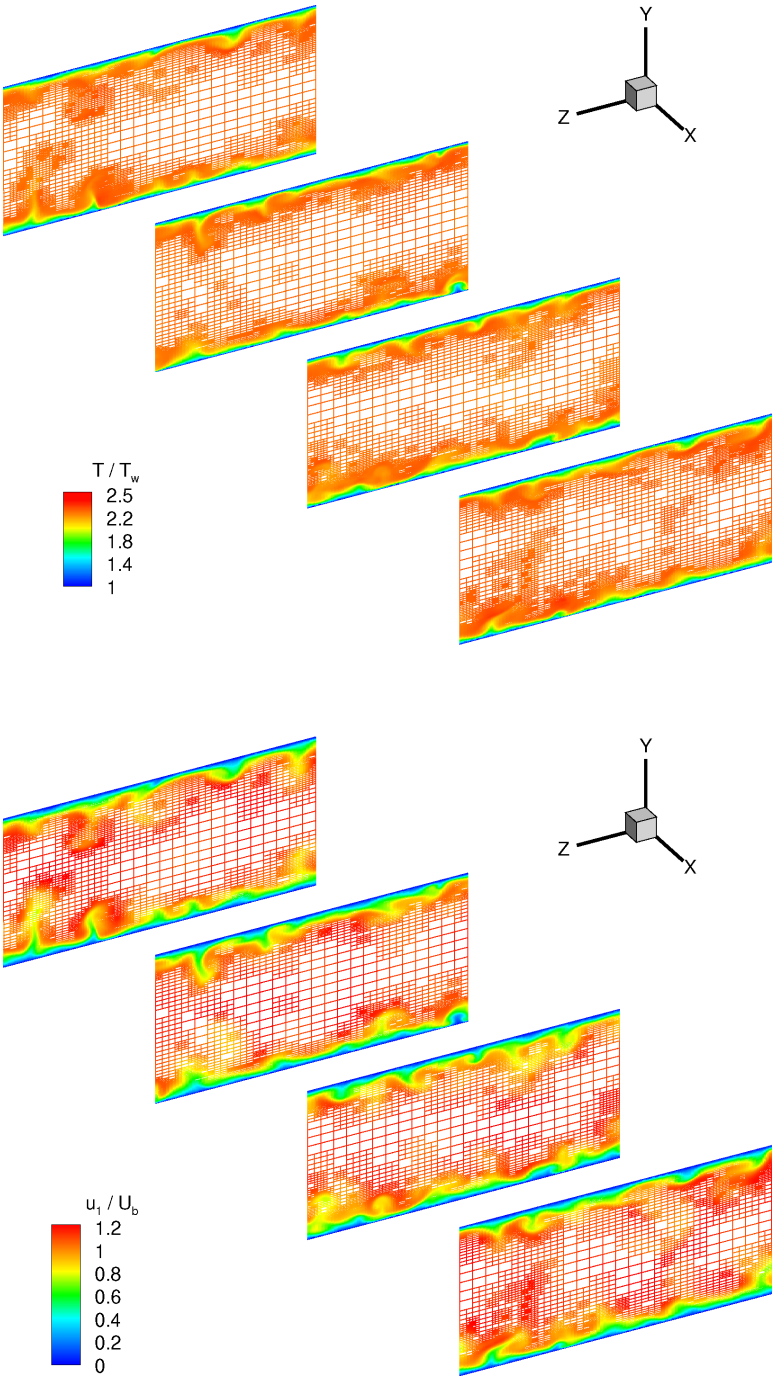

FIG. 1. Instantaneous adaptive mesh colored by normalized temperature (top) and streamwise velocity (bottom) contours, for four different equispaced cross-sections of the channel.

TABLE I. Numerical resolution, grid compression and mean flow results for WA-LES, LES and DNS.

Method	Resolution	Compression	Δx_1^+	$\Delta x_{2,w}^+$	Δx_3^+	Re_τ	Ma_τ	$-B_q$	u_c/U_b	T_c/T_w	ρ_c/ρ_w
WA-LES (LDKM)	$132 \times 177 \times 132$	96%	41.1	0.12	13.7	432	0.113	0.13	1.18	2.37	0.42
WA-LES (AMD)	$141 \times 95 \times 94$	95%	40.8	0.13	20.4	458	0.107	0.13	1.20	2.69	0.37
LES [45]	$128 \times 65 \times 81$	0%	45	0.23	23.7	459	0.112	0.14	1.2	2.67	—
DNS [35]	$144 \times 119 \times 80$	0%	39	0.2	24	451	0.116	0.137	1.17	2.49	0.40

and temperature are determined as $u_\tau = (\tau_\mathrm{w}/\rho_\mathrm{w})^{1/2}$ and $T_\tau = -q_\mathrm{w}/(\rho_\mathrm{w} c_p u_\tau)$, where ρ_w and q_w represent the wall-averaged density and the wall heat flux. The present results for compressible WA-LES with LDKM are compared with the reference studies, namely, the DNS in Ref. [35], the nonadaptive LES in Ref. [45], and the WA-LES based on AMD model in Ref. [33].

B. Simulation settings

WA-LES solution for the above benchmark flow is attained by employing the parallel version of the wavelet-based solver [52], using the fourth-order A-AWC method supplied with the linearized Crank–Nicolson split-step time integration method with adaptive time stepping. The number of resolution levels in the wavelet decomposition Eq. (2) is fixed to $J_\mathrm{max} = 8$, with the coarsest and the finest adaptive rectilinear grids consisting of $48 \times 65 \times 48$ and $768 \times 1025 \times 768$ wavelets, respectively. As permitted by the A-AWC approach, uniform grids are used in the computational space, whereas the corresponding meshes in the physical domain are stretched in the wall-normal direction, following a hyperbolic tangent distribution. Since the minimum mesh spacing in the wall-normal direction that is $\Delta Y_w/H = 2.9 \times 10^{-4}$ results in being even smaller than that used for DNS [35], the present simulation can be referred to as wall-resolved WA-LES. Note that, for the efficient parallel implementation of the simulation, an octree type wavelet collocation grid has been employed for wavelet coefficients storage, retrieval, and parallel data migration. In addition, a dynamic load balancing algorithm has been implemented via domain repartitioning during the grid adaptation step and reassigning tree data structure nodes to the appropriate processors.

To adequately capture both kinematically and thermodynamically significant phenomena, the grid adaptation is performed based on all the resolved variables. Only a low fraction of the total number of available wavelets is actually employed in the simulation, depending on the wavelet thresholding level that is used. As demonstrated in past studies, the choice of the uniform level of thresholding is very important, especially if no explicit filtering operation is performed and the pure built-in filtering effect of the wavelet-based grid adaptation is used [53]. Here, also based on past

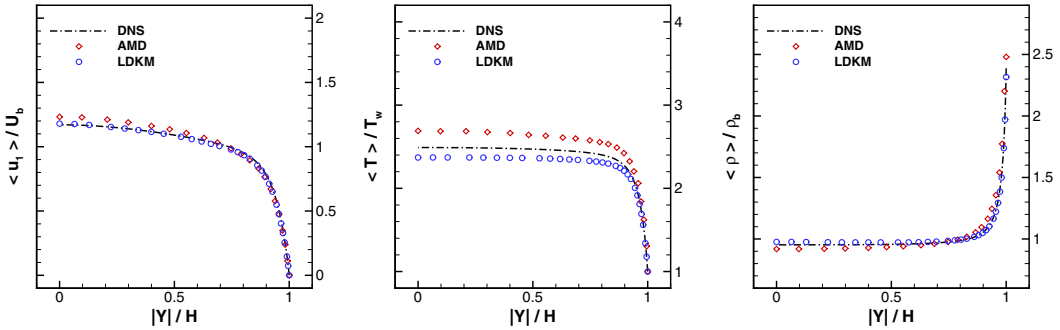

FIG. 2. Normalized mean streamwise velocity (left), temperature (middle) and density (right) for WA-LES solutions, compared to reference DNS [35].

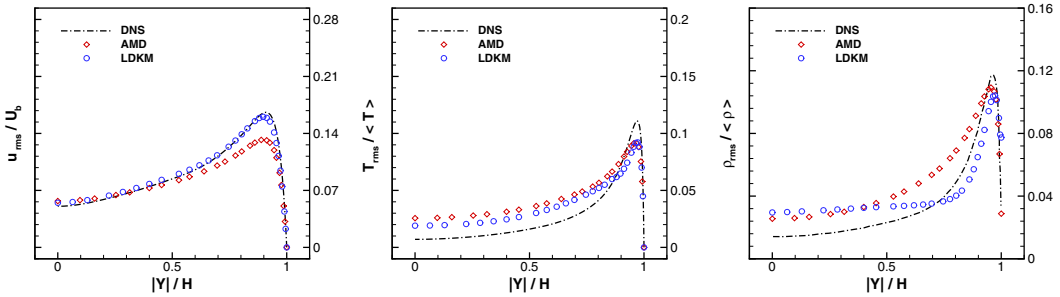

FIG. 3. Normalized RMS values of streamwise velocity (left), temperature (middle), and density (right) fluctuations for WA-LES solutions, compared to reference DNS [35].

WA-LES studies, this parameter is selected as $\epsilon = 5 \times 10^{-2}$, which represents a fair compromise between desired turbulence resolution, necessary numerical accuracy, and acceptable computational cost. The model coefficients for the LDKM procedure are dynamically evaluated as discussed in Section IV, where the test-filtering operation is performed with $\alpha = 2$.

C. Results

To illustrate the instantaneous resolved flow field, the adapted grid is shown in Fig. 1, together with the contours of normalized temperature and streamwise velocity, for four different cross-sections equispaced along the channel. Apparently, the actual mesh consists of a very low fraction of the available grid points, being refined around localized flow structures. In fact, the high grid compression that is achieved in the present case is comparable to that found in past WA-LES studies of wall-bounded turbulent flows, for both incompressible [32] and compressible [33] cases.

The present mesh spacings, expressed in viscous wall units, are provided in Table I, together with some mean flow results. These data show a very good agreement of the integral flow characteristics in comparison to reference data, with the friction Reynolds number being slightly underestimated. Following Ref. [33], instead of reporting the numerical resolution corresponding to the finest grid that is occasionally employed in WA-LES, the resolution corresponding to a reference, say equivalent, nonadaptive grid is shown. The equivalent grid is defined by not altering the relative number of points along the three spatial directions, while approximately matching the overall number of retained grid points. This way, a more meaningful comparison between WA-LES and reference nonadaptive resolutions is achieved in the homogeneous directions. Unfortunately, this is not true for the nonhomogeneous wall-normal direction, for which, more appropriately, the minimum mesh spacing close to the walls is provided. Note that finer spatial resolution is permitted in the spanwise direction with respect to DNS, where a higher order numerical approach using a Fourier-Legendre

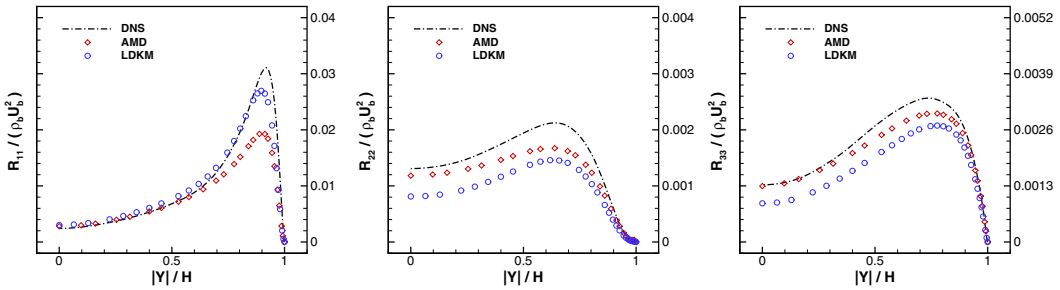

FIG. 4. Resolved turbulent normal stresses for WA-LES solutions, compared to reference DNS [35].

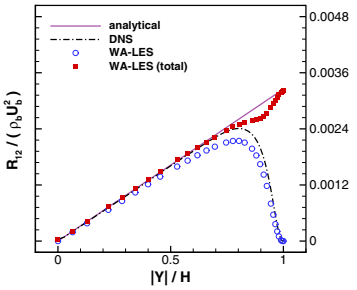

FIG. 5. Turbulent shear stress, compared to reference DNS [35].

spectral discretization was utilized [35]. In practice, the number of retained wavelets on the highest levels of resolution is very low and the corresponding finest spatial grids are used only in very limited flow regions. This is demonstrated by the achieved grid compression that is measured as the percentage of discarded grid points with respect to the nominally available ones. Here, since the finest collocation grid is very seldom involved in the calculation, the grid compression reported in Table I is measured at the highest but one level of resolution ($j = J_{\max} - 1$).

It should be emphasized that the appearance of intermittently occurring regions of high resolution, as illustrated in Fig. 1 for the present case, indicates the existence of localized energy–containing/dynamically important coherent turbulent eddies, whose relative importance is controlled by the WTF level. This fact is consistent with the results of high-fidelity turbulence simulations, where the rare occurrence of strong eddy structures at scales even smaller than the Kolmogorov scale was observed [54,55]. In the context of classical lowpass filter-based LES, the reduction of the local mesh resolution would predetermine the smallest allowable scales and dynamically important structures would need to be dissipated by the SGS mdel. For WA-LES, a similar reduction of the turbulence resolution can also be achieved by increasing the level of thresholding, as was discussed in details in Ref. [33].

Once fully developed turbulent flow conditions are achieved, the mean flow variables can be evaluated as Reynolds-averaged fields, by employing a long-time averaging procedure conducted over several flow-through times, along with spatial averaging in the homogeneous plane. Note that, after having double checked the mean flow symmetry with respect to the channel midplane, the reported flow statistics are obtained by further averaging the sampled data on the two sides of the channel. In the following discussion, the mean variables are denoted by angular brackets, while primed quantities stand for the corresponding fluctuations. Some mean flow variables of interest are illustrated in Fig. 2, where the profiles across the channel of normalized streamwise velocity, temperature and density are reported. The overall comparison with reference DNS data [35] is quite satisfying. To demonstrate the ability of the WA-LES approach to adequately predict turbulent

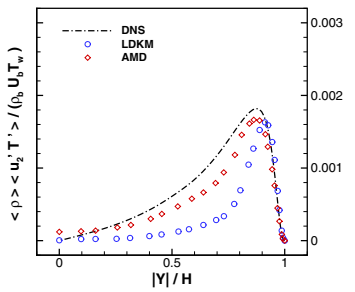

FIG. 6. Resolved turbulent heat flux for WA-LES solutions, compared to reference DNS [35].

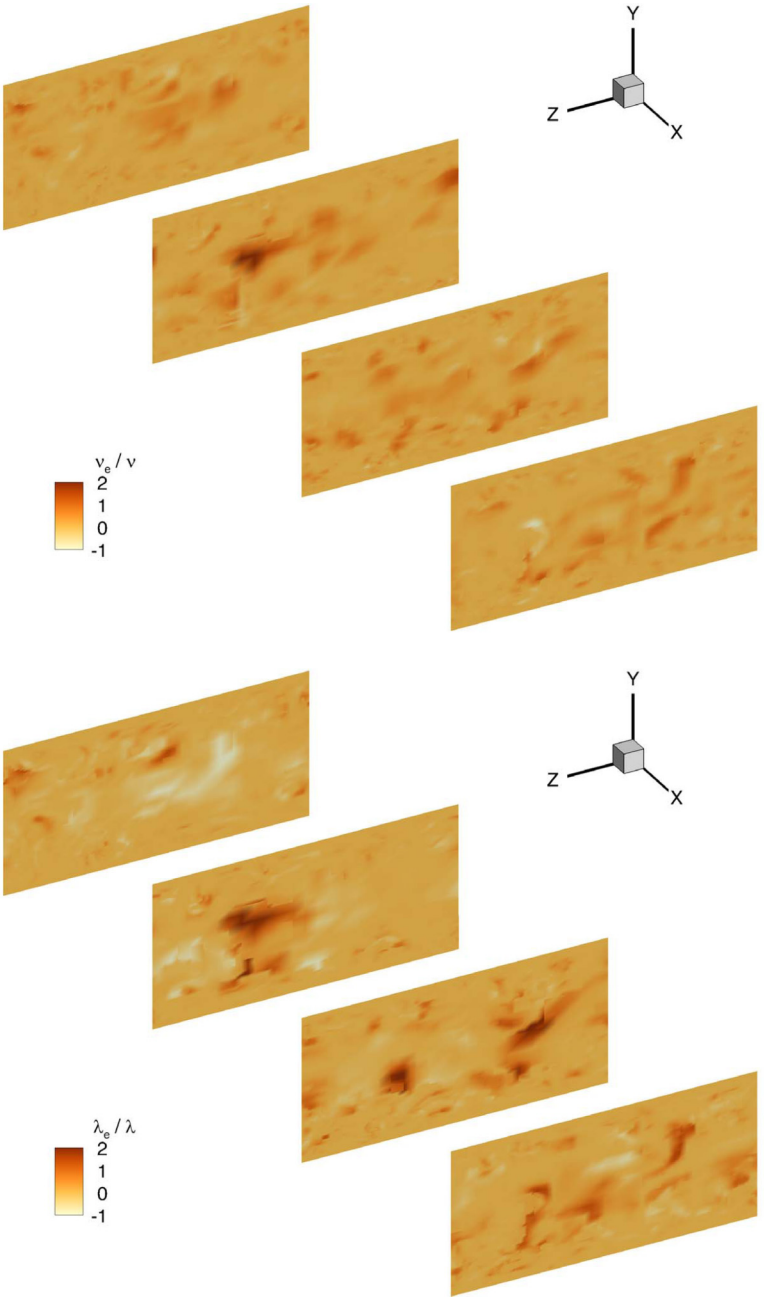

FIG. 7. Instantaneous contour maps of viscosity (top) and conductivity (bottom) ratios, for four different equispaced cross-sections of the channel.

fluctuations in the resolved variables, the normalized root-mean-square (RMS) values of the same variables are depicted in Fig. 3. The fluctuations are slightly overestimated in the central region of the channel. However, the present results are consistent with traditional nonadaptive LES [45].

Furthermore, the WA-LES solution is analyzed in terms of resolved turbulent stresses that are $\mathcal{R}_{ij} = \langle \overline{\rho}^{>\epsilon} u_i' u_j' \rangle$, where $u_i' = \widetilde{u}_i - \langle \widetilde{u}_i \rangle$. The resolved normal stresses, which are drawn in Fig. 4,

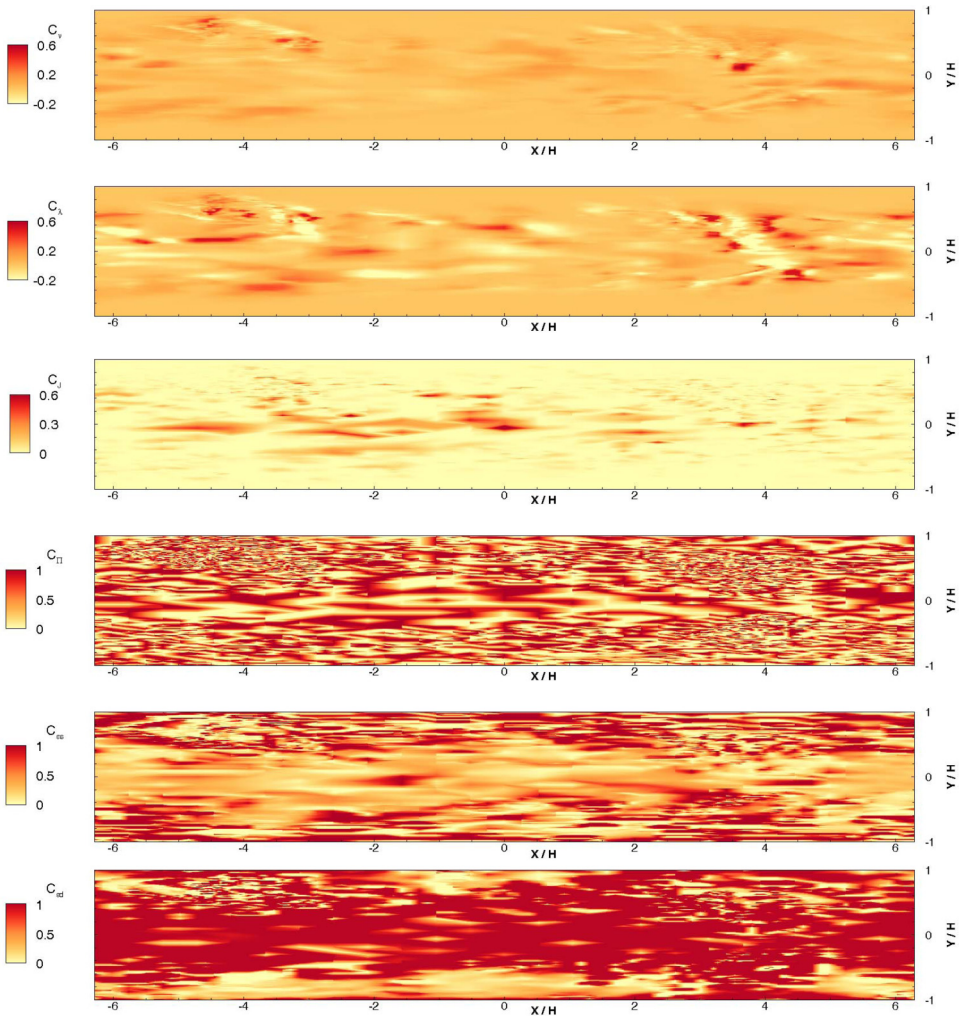

FIG. 8. Instantaneous contour maps of the dynamic model coefficients that are C_ν, C_λ, C_J, C_Π, C_{ε_s}, and C_{ε_d} at the channel midplane.

show good agreement with the reference DNS data [35], with the location of the peaks, corresponding to the turbulence-producing regions close to the walls, being well predicted. Apparently, the resolved turbulent stresses in WA-LES are generally lower than found in DNS, because the energy content of the discarded wavelet modes is however nonnegligible, with the SGS contribution being responsible for approximating the differences. As far as the turbulent shear stress is concerned, the total stress that is the sum of resolved turbulent shear stress, viscous shear stress and modeled SGS shear stress,

$$\mathcal{R}_{12}^{\mathrm{tot}} = \langle \overline{\rho}^{>\epsilon} \widetilde{u}_1 \widetilde{u}_2 \rangle + \left\langle -\widetilde{\mu} \frac{\partial \widetilde{u}_1}{\partial x_2} \right\rangle + \left\langle -\overline{\rho}^{>\epsilon} \nu_e \frac{\partial \widetilde{u}_1}{\partial x_2} \right\rangle, \tag{76}$$

is reported in Fig. 5. When making a comparison with the resolved stress in DNS, the effect of LDKM in approximating the unresolved part of the turbulent shear stress in WA-LES is apparent. Similarly to turbulent stresses, the turbulent heat flux is partly resolved by the WA-LES solution, as illustrated in Fig. 6, where the profile of $\langle \overline{\rho}^{>\epsilon} \rangle \langle u_2' T' \rangle$ is drawn.

It should be pointed out that, even though the results of WA-LES based on LDKM and AMD models are in good agreement with each other and DNS data, there are some distinct differences in the higher order statistics that originate from the different nature of the closing procedures. Contrarily to the LDKM approach, where the evolution of the SGS energy is explicitly simulated by solving the associated transport equation, the AMD model imposes a balance of production and dissipation of SGS energy at the local grid scale [56]. The above discrepancy is thus not surprising, taking into account that SGS models directly affect what part of the turbulent flow structures is resolved and what part is modeled. Indeed, the analysis of WA-LES statistics with respect to DNS should be used to highlight the difference in modeling approaches and not to make a direct comparison between partially and fully resolved turbulent flow simulations. For instance, as can be seen in Fig. 4, the longitudinal turbulent stress is better resolved by LDKM, while AMD better captures normal and transverse turbulent stresses. This is due to the more robust handling of the flow anisotropy by the AMD model, compared to the isotropic nature of the Smagorinsky-type approximation Eq. (50) employed by the LDKM procedure. A similar discussion could be made for the turbulent fluctuations reported in Fig. 3, as well as the turbulent heat flux in Fig. 6.

Finally, to demonstrate the importance of the modeled residual terms in WA-LES with LDKM, the ratios of turbulent eddy-viscosity and eddy-conductivity to corresponding molecular values, namely, $\nu_e/\widetilde{\nu}$ (where $\widetilde{\nu} = \widetilde{\mu}/\overline{\rho}^{\mathcal{>}\epsilon}$) and $\lambda_e/\tilde{\lambda}$, are examined. The instantaneous contours of these variables are reported in Fig. 7, at the same time instant and for the same four different cross-sections considered in Fig. 1. The present values of these ratios are perfectly consistent with previous findings for both incompressible and compressible WA-LES [20,33]. It is worth stressing that the modeled SGS terms provided by the LDKM procedure automatically converge to zero at the walls, where the eddy-viscosity and the eddy-conductivity vanish. The localized dynamic character of the proposed model is further illustrated in Fig. 8, where the instantaneous contours of the six different model coefficients are drawn, for instance, at the midplane of the channel.

VI. CONCLUSIONS

The use of localized closure models is essential for the application of compressible WA-LES to inhomogeneous flows. In this work, a new dynamic model based on the solution of the additional transport equation for the SGS kinetic energy is originally introduced and developed. The various residual terms appearing in the wavelet-filtered governing equations are individually modeled by means of either Germano-like or Bardina-like dynamic procedures. This way, differently from other SGS modeling approaches involving the use of *a priori* prescribed model coefficients, including the reference AMD model, the proposed LDKM leads to a self-closed procedure.

The results obtained for a classical benchmark flow that is the supersonic plane channel with isothermal walls show that the localized dynamic kinetic-energy model can be successfully used for closing the compressible WA-LES governing equations. Both accuracy and efficiency of the solution are demonstrated, making a comparison with conventional nonadaptive LES and DNS. Moreover, based on the present application results, the accuracy of the resolved turbulent fluctuations in the wall region demonstrates an important feature of the compressible WA-LES method. Due to the automatic adaptation process, the presence of high gradients in the mean flow field variables, along with significant turbulent fluctuations, results in using locally finer grid resolution close to the walls. This fact leads to the retention of energy for the high wavenumber modes and the corresponding increased local resolution with respect to conventional lowpass filter-based nonadaptive LES. In contrast, in the central region of the channel, due to the slowly spatially varying mean flow and less significant turbulence, coarser grids are employed in the calculation, which results in the inferior resolution. In the future, it would be beneficial to study the performance of WA-LES with LDKM in complex external flow scenarios [57].

It should be noted that the compressible WA-LES method discussed in this paper has to be distinguished from the recently proposed compressible LES with adaptive mesh refinement (AMRLES) [27], where ad hoc gradient-based adaptive block-structured mesh refinement is used

for better resolution of the flow regions near the shocks, rather than capturing and resolving the energetic coherent turbulent structures on the dynamically adaptive computational mesh as in the present formulation. Also, it is worth stressing that the present WA-LES approach exploits the wavelet collocation method for solving the wavelet-filtered governing equations, differently from lower-fidelity approaches, where the same method was limited to the efficient solution of differently modeled equations. However, together with the wavelet-based adaptive unsteady RANS recently developed in Refs. [58–60], the present wall-resolved WA-LES formulation paves the way for further development of the wavelet-based adaptive eddy-resolving method for modeling and simulation of complex wall-bounded compressible turbulent flows [61].

ACKNOWLEDGMENTS

The authors acknowledge the CINECA awards under the ISCRA initiative (Projects No. HP10CTESFT and No. HP10BSBCBZ) for the availability of high-performance computing resources.

[1] D. C. Wilcox, *Turbulence Modeling for CFD* (DCW Industries, La Canada, CA, 2006).
[2] P. A. Durbin and B. A. Pettersson-Reif, *Statistical Theory and Modeling for Turbulent Flow* (John Wiley & Sons, Hoboken, NJ, 2011).
[3] P. A. Durbin, Some recent developments in turbulence closure modeling, Annu. Rev. Fluid Mech. **50**, 77 (2018).
[4] M. Germano, U. Piomelli, P. Moin, and W. H. Cabot, A dynamic subgrid-scale eddy viscosity model, Phys. Fluids **3**, 1760 (1991).
[5] M. Lesieur and O. Métais, New trends in large-eddy simulations of turbulence, Annu. Rev. Fluid Mech. **28**, 45 (1996).
[6] C. Meneveau and J. Katz, Scale-invariance and turbulence models for large-eddy simulation, Annu. Rev. Fluid Mech. **32**, 1 (2000).
[7] U. Piomelli and E. Balaras, Wall-layer models for large-eddy simulations, Annu. Rev. Fluid Mech. **34**, 349 (2002).
[8] J. Larsson, S. Kawai, J. Bodart, and I. Bermejo-Moreno, Large eddy simulation with modeled wall-stress: Recent progress and future directions, Mech. Eng. Rev. **3**, 15-00418 (2016).
[9] S. T. Bose and G. I. Park, Wall-modeled large-eddy simulation for complex turbulent flows, Annu. Rev. Fluid Mech. **50**, 535 (2018).
[10] P. R. Spalart, S. Deck, M. L. Shur, K. D. Squires, M. K. Strelets, and A. K. Travin, A new version of detached-eddy simulation, resistant to ambiguous grid densities, Theor. Comput. Fluid Dyn. **20**, 181 (2006).
[11] M. L. Shur, P. R. Spalart, M. K. Strelets, and A. K. Travin, Detached-eddy simulation of an airfoil at high angle of attack, Eng. Turbul. Model. Exper. **4**, 669 (1999).
[12] H. Zhao, A. Uzun, M. Y. Hussaini, and S. L. Woodruff, Computations of flow past a circular cylinder using a continuous-turbulence model, AIAA J. **47**, 2460 (2009).
[13] M. L. Shur, P. R. Spalart, M. K. Strelets, and A. K. Travin, A hybrid RANS-LES approach with delayed-DES and wall-modelled LES capabilities, Int. J. Heat Fluid Flow **29**, 1638 (2008).
[14] J. Fröhlich and D. von Terzi, Hybrid LES/RANS methods for the simulation of turbulent flows, Progr. Aerospace Sci. **44**, 349 (2008).
[15] H. Xiao and P. Jenny, A consistent dual-mesh framework for hybrid LES/RANS modeling, J. Comput. Phys. **231**, 1848 (2012).
[16] P. Moin and K. Mahesh, Direct numerical simulation: A tool in turbulence research, Annu. Rev. Fluid Mech. **30**, 539 (1998).
[17] H. Choi and P. Moin, Grid-point requirements for large eddy simulation: Chapman's estimates revisited, Phys. Fluids **24**, 011702 (2012).

[18] G. De Stefano, O. V. Vasilyev, and D. E. Goldstein, *A priori* dynamic test for deterministic/stochastic modeling in large-eddy simulation of turbulent flow, Comput. Phys. Commun. **169**, 210 (2005).
[19] D. E. Goldstein and O. V. Vasilyev, Stochastic coherent adaptive large eddy simulation method, Phys. Fluids **16**, 2497 (2004).
[20] G. De Stefano and O. V. Vasilyev, A fully adaptive wavelet based approach to homogeneous turbulence simulation, J. Fluid Mech. **695**, 149 (2012).
[21] G. De Stefano and O. V. Vasilyev, Hierarchical adaptive eddy-capturing approach for modeling and simulation of turbulent flows, Fluids **6**, 83 (2021).
[22] G. De Stefano, A. Nejadmalayeri, and O. V. Vasilyev, Wall-resolved wavelet-based adaptive large-eddy simulation of bluff-body flows with variable thresholding, J. Fluid Mech. **788**, 303 (2016).
[23] P. Moin, K. Squires, W. Cabot, and S. Lee, A dynamic subgrid-scale model for compressible turbulence and scalar transport, Phys. Fluids **3**, 2746 (1991).
[24] N. Park and K. Mahesh, Numerical and modeling issues in LES of compressible turbulence on unstructured grids, *45th AIAA Aerospace Sciences Meeting and Exhibit*, January 8–11, Reno, Nevada, 2007.
[25] F. Génin and S. Menon, Dynamics of sonic jet injection into supersonic cross-flow, J. Turbul. **11**, N4 (2010).
[26] X. Chai and K. Mahesh, Dynamic-equation model for large-eddy simulation of compressible flows, J. Fluid Mech. **699**, 385 (2012).
[27] B. Muralidharan and S. Menon, A consistent multilevel subgrid scale closure for large eddy simulation of compressible flow using adaptive mesh refinement, Comput. Fluids **180**, 159 (2019).
[28] O. V. Vasilyev, G. De Stefano, D. E. Goldstein, and N. K.-R. Kevlahan, Lagrangian dynamic SGS model for stochastic coherent adaptive large eddy simulation, J. Turbul. **9**, N11 (2008).
[29] G. De Stefano, O. V. Vasilyev, and D. E. Goldstein, Localized dynamic kinetic-energy-based models for stochastic coherent adaptive large eddy simulation, Phys. Fluids **20**, 045102 (2008).
[30] G. De Stefano and O. V. Vasilyev, Stochastic coherent adaptive large eddy simulation of forced isotropic turbulence, J. Fluid Mech. **646**, 453 (2010).
[31] A. Nejadmalayeri, A. Vezolainen, G. De Stefano, and O. V. Vasilyev, Fully adaptive turbulence simulations based on Lagrangian spatiotemporally varying wavelet thresholding, J. Fluid Mech. **749**, 794 (2014).
[32] G. De Stefano and O. V. Vasilyev, Wavelet-based adaptive simulations of three-dimensional flow past a square cylinder, J. Fluid Mech. **748**, 433 (2014).
[33] G. De Stefano, E. Brown-Dymkoski, and O. V. Vasilyev, Wavelet-based adaptive large-eddy simulation of supersonic channel flow, J. Fluid Mech. **901**, A13 (2020).
[34] W. Rozema, H.J. Bae, P. Moin, and R. Verstappen, Minimum-dissipation models for large-eddy simulation, Phys. Fluids **27**, 085107 (2015).
[35] G.N. Coleman, J. Kim, and R.D. Moser, A numerical study of turbulent supersonic isothermal-wall channel flow, J. Fluid Mech. **305**, 159 (1995).
[36] B. Vreman, B. Geurts, and H. Kuerten, *A priori* tests of large eddy simulation of compressible plane mixing layer, J. Eng. Math. **29**, 299 (1995).
[37] E. Garnier, N. Adams, and P. Sagaut, *Large Eddy Simulation for Compressible Flows* (Springer, Berlin, 2009).
[38] M. Pino Martín, U. Piomelli, and G.V. Candler, Subgrid-scale models for compressible large-eddy simulations, Theoret. Comput. Fluid Dyn. **13**, 361 (2000).
[39] O. V. Vasilyev, Solving multidimensional evolution problems with localized structures using second generation wavelets, Int. J. Comput. Fluid Dyn. **17**, 151 (2003).
[40] E. Brown-Dymkoski and O. V. Vasilyev, Adaptive-anisotropic wavelet collocation method on general curvilinear coordinate systems, J. Comput. Phys. **333**, 414 (2017).
[41] W. Sweldens, The lifting scheme: A construction of second generation wavelets, SIAM J. Math. Anal. **29**, 511 (1998).
[42] S. Ghosal, T.S. Lund, P. Moin, and K. Akselvoll, A dynamic localization model for large-eddy simulation of turbulent flows, J. Fluid Mech. **286**, 229 (1995).
[43] C.G. Speziale, Analytic methods for the development of Reynolds-stress closures in turbulence, Annu. Rev. Fluid Mech. **23**, 107 (1991).

[44] B. Vreman, B. Geurts, and H. Kuerten, Subgrid-modeling in LES of compressible flow, Appl. Sci. Res. **54**, 191 (1995).
[45] C. Brun, M. Petrovan Boiarciuc, M. Haberkorn, and P. Comte, Large eddy simulation of compressible channel flow, Theor. Comput. Fluid Dyn. **22**, 189 (2008).
[46] S. Sarkar, G. Erlebacher, M. Y. Hussaini, and H. O. Kreiss, The analysis and modelling of dilatational terms in compressible turbulence, J. Fluid Mech. **227**, 473 (1991).
[47] D.K. Lilly, A proposed modification of the Germano subgrid-scale closure method, Phys. Fluids **4**, 633 (1992).
[48] J. Wang, M. Wan, S. Chen, and S. Chen, Kinetic-energy transfer in compressible isotropic turbulence, J. Fluid Mech. **841**, 581 (2018).
[49] S. Menon and W.-W. Kim, High Reynolds number flow simulations using the localized dynamic subgrid-scale model, in *Proceedings of the 34th AIAA Aerospace Sciences Meeting and Exhibit*, Reno, NV (1996).
[50] E. Pomraning and C.J. Rutland, Dynamic one-equation nonviscosity large-eddy simulation model, AIAA J. **40**, 689 (2002).
[51] P.G. Huang, G.N. Coleman, and P. Bradshaw, Compressible turbulent channel flows: DNS results and modelling, J. Fluid Mech. **305**, 185 (1995).
[52] A. Nejadmalayeri, A. Vezolainen, E. Brown-Dymkoski, and O. V. Vasilyev, Parallel adaptive wavelet collocation method for PDEs, J. Comput. Phys. **298**, 237 (2015).
[53] G. De Stefano and O. V. Vasilyev, Wavelet-based adaptive large eddy simulation with explicit filtering, J. Comput. Phys. **238**, 240 (2013).
[54] V. Yakhot and K.R. Sreenivasan, Anomalous scaling of structure functions and dynamic constraints on turbulence simulations, J. Stat. Phys. **121**, 823 (2005).
[55] A. Nejadmalayeri, A. Vezolainen, and O. V. Vasilyev, Reynolds number scaling of coherent vortex simulation and stochastic coherent adaptive large eddy simulation, Phys. Fluids **25**, 110823 (2013).
[56] W. Rozema, R .W. C. P. Verstappen, A. E. P. Veldman, and J. C. Kok, Low-dissipation simulation methods and models for turbulent subsonic flow, Arch. Comput. Methods Eng. **27**, 299 (2020).
[57] N. Kasimov, E. Dymkoski, G. De Stefano, and O. V. Vasilyev, Galilean-invariant characteristic-based volume penalization method for supersonic flows with moving boundaries, Fluids **6**, 293 (2021).
[58] G. De Stefano, O. V. Vasilyev, and E. Brown-Dymkoski, Wavelet-based adaptive unsteady Reynolds-averaged turbulence modelling of external flows, J. Fluid Mech. **837**, 765 (2018).
[59] X. Ge, O. V. Vasilyev, G. De Stefano, and M. Y. Hussaini, Wavelet-based adaptive unsteady Reynolds-averaged Navier-Stokes computations of wall-bounded internal and external compressible turbulent flows, in *2018 AIAA Aerospace Sciences Meeting* (Kissimmee, Florida, 2018).
[60] X. Ge, O. V. Vasilyev, G. De Stefano, and M. Y. Hussaini, Wavelet-based adaptive unsteady Reynolds-averaged Navier-Stokes simulations of wall-bounded compressible turbulent flows, AIAA J. **58**, 1529 (2020).
[61] X. Ge, G. De Stefano, M. Y. Hussaini, and O. V. Vasilyev, Wavelet-based adaptive eddy-resolving methods for modeling and simulation of complex wall-bounded compressible turbulent flows, Fluids **6**, 331 (2021).